ARTICLE

Aqueous Solution Synthesis of CaF_2 Hollow Microspheres via the Ostwald Ripening Process at Room Temperature

Wen-Shou Wang, Liang Zhen,* Cheng-Yan Xu, Jun-Zhou Chen, and Wen-Zhu Shao

School of Materials Science and Engineering, Harbin Institute of Technology, Harbin 150001, People's Republic of China

ABSTRACT Nearly monodispersive CaF_2 hollow microspheres were synthesized by a facile aqueous solution route from the mixed aqueous solutions of $CaCl_2$, Na_2WO_4, and NaF at room temperature. The as-prepared products were characterized by X-ray diffraction (XRD), scanning electron microscopy, transmission electron microscopy (TEM), high-resolution transmission electron microscopy, and N_2 adsorption−desorption techniques. The CaF_2 hollow microspheres have an average diameter of about 1.5 μm and a hollow interior of 0.5 μm. The shell is composed of numerous single-crystalline nanoparticles with diameter of about 20 nm. The morphologies and diameters of the CaF_2 products are strongly dependent on the experimental parameters, such as the concentration of the aqueous NaF solution and the reaction temperature. The synthetic experiments indicate that the growth process of CaF_2 hollow microspheres involves first the formation of $CaWO_4$ solid microspheres and then the formation of CaF_2 solid microspheres through the reaction between $CaWO_4$ and F^- ions controlled by the difference of the solubility product for $CaWO_4$ and CaF_2. Phenomenological elucidation based on TEM observations and XRD patterns of intermediate products at different precipitation stages indicates that the formation mechanism for the CaF_2 hollow microspheres is related to the Ostwald ripening mechanism. N_2 adsorption−desorption measurement shows that the CaF_2 hollow microspheres possess a high Brunauer−Emmett−Teller surface area and porosity properties. The synthetic procedure is straightforward and represents a new example of the Ostwald ripening mechanism for the formation of inorganic hollow structures in an aqueous solution at room temperature.

KEYWORDS: hollow microspheres • Ostwald ripening • calcium fluoride • chemical conversion

1. INTRODUCTION

Hollow inorganic micro- and nanostructures with defined shape and composition have recently attracted fascinating attention because of their promising applications in various fields, such as nanoscale chemical reactors, efficient catalysts, drug-delivery catties, active-material encapsulation, energy-storage media, photonic building blocks, and so forth (1). Especially, hollow nano/microspheres with porous shells would exhibit more advantages in mass diffusion and transportation compared with conventional hollow spheres with solid shells. Until now, the general strategy for the synthesis of hollow nano/microspheres is based on a template-assisted process involving the use of various removable templates, including monodispersive silica (2), polymer latex spheres (3), and carbon spheres (4), and the reduction of metal nanoparticles (5) as hard templates and emulsion droplets and/or micelles (6−9), liquid drops (10), vesicles (11), and even gas bubbles (12) as soft templates. Following these procedures, the templates are first coated with the desired materials to obtain core−shell structures, and then the templates are removed by a time-consuming treatment such as calcination at high temperature or dissolution with appropriate solvents to form hollow structures. In some cases, the yield of hollow spheres synthesized through the template-assisted methods is low or their shells are not intact, which usually leads to poor mechanical performance. Therefore, the main task will be to explore other template-free strategies, aiming at a facile "one-step" synthetic approach for hollow structures. Recently, utilization of the well-known classical physical phenomenon Ostwald ripening mechanism provides an optional opportunity for the fabrication of hollow structures (13). Since application of the Ostwald ripening mechanism in the fabrication of inorganic hollow nanostructures was proposed for the first time in the synthesis of TiO_2 nanospheres reported by Zeng et al. (14), this process is believed to be promising for a broad range of inorganic materials. However, fabrication of inorganic hollow structures based on the Ostwald ripening mechanism has been lingering far behind comparison with the great progress in templated synthesis. Therefore, developing facile Ostwald ripening mechanism-based methods is still highly desired for a more generic fabrication of many inorganic hollow structures with controlled composition, shape, and size.

Alkaline-earth metal fluorides (MF_2, M = Ca, Sr, and Ba) are dielectric and thus widely used in microelectric and optoelectric devices, such as wide-gap insulating overlayers, gate dielectrics, insulators, and buffer layers in semiconductor-on-insulator structures and more advanced 3D devices (15). As one of the most important alkaline-earth metal fluorides, calcium fluoride (CaF_2) has attracted increasing interest with respect to various applications in UV lithography, UV-transparent optical lenses, and the surface conditioning of glass, as promoting agents for bone/teeth recon-

* Corresponding author. E-mail: lzhen@hit.edu.cn.
Received for review November 30, 2008 and accepted March 12, 2009

DOI: 10.1021/am8002044

Published on Web 04/01/2009

struction, as biocompatible luminescent markers, etc. (16). To date, various nanostructures of CaF_2, such as nanoparticles, nanocubes, and nanorods have been extensively synthesized by a polyol-mediated method (17a), a hydrothermal/solvothermal process (17b, 17c), and an ambient template-directed route (17d). Despite these advances, the diversity of the desired geometry for CaF_2 nanostructures still needs to be greatly expanded to meet the future nanotechnological demand. However, to the best of our knowledge, there has been no research work reported concerning the synthesis of CaF_2 hollow microspheres by a template-free method. Therefore, the synthesis of CaF_2 hollow microspheres by a convenient aqueous solution route, especially at room temperature, is still a challenge for materials science and chemistry that needs to be addressed.

Recently, we have demonstrated a facile room temperature aqueous solution method for the synthesis of ternary metal oxide inorganic nanostructures without using any templates or surfactant (18). These results have inspired us to combine the "room temperature aqueous solution route" and the "Ostwald ripening mechanism", which may realize the invention of room temperature synthesis of inorganic structures with hollow interiors based on the Ostwald ripening mechanism. In this work, we developed a simple aqueous solution for the synthesis of CaF_2 hollow microspheres with mesopores on the shells from the mixed aqueous solutions of $CaCl_2$, Na_2WO_4, and NaF at room temperature. The shells of the hollow microspheres consisted of numerous single-crystalline nanoparticles 20 nm in size. The effects of various reaction conditions on the morphology and size of CaF_2 products, such as the concentration of the aqueous NaF solution and the reaction temperature, are also investigated. The controlled synthetic experiments indicate that the formation process of CaF_2 hollow microspheres involves first the formation of $CaWO_4$ solid microspheres and then the growth of CaF_2 solid microspheres through the reaction between $CaWO_4$ and F^- ions controlled by the difference of the solubility products (K_{sp}) for $CaWO_4$ and CaF_2. The Ostwald ripening mechanism was proposed to account for the formation of hollow microspheres on the basis of transmission electron microscopy (TEM) observations of intermediate products at different precipitation stages. In addition, the specific surface area and pore-size distribution of the obtained CaF_2 hollow microspheres are also investigated by the N_2 adsorption–desorption method, which shows that the CaF_2 hollow microspheres possess a high Brunauer–Emmett–Teller (BET) surface area and porosity properties. The results may represent a new example of Ostwald ripening mechanism-based formation of inorganic hollow structures in the template-free aqueous solution at room temperature. We expect that these CaF_2 hollow microspheres with porous shells may open the doors for finding new properties and applications with respect to their bulk counterparts and/or enhancing the performance of currently existing devices. For example, the hollow interior of CaF_2 microspheres can act as a good container for many functional guest materials, while the interstitials between the sphere's shells will enable guest materials traveling in or out to work as "nanochannels" for material exchange between the interior and exterior of the spheres (11, 19).

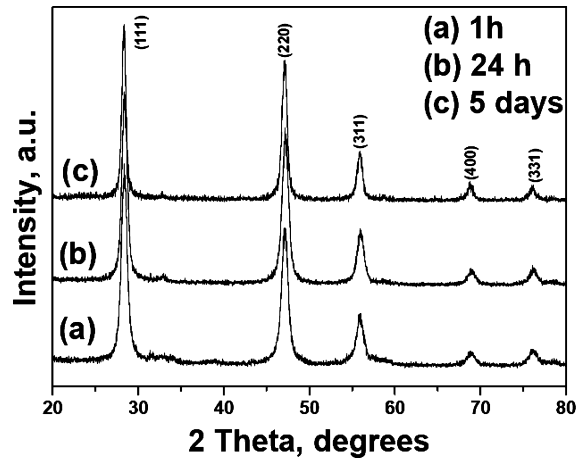

FIGURE 1. XRD patterns of the as-synthesized CaF_2 microspheres with different reaction times, with the other reaction conditions remaining the same: (a) 1 h, (b) 24 h; (c) 5 days.

2. EXPERIMENTAL SECTION

All chemicals were of analytical grade and were used as received without further purification. In a typical experiment, 5.0 mmol of $Na_2WO_4 \cdot 2H_2O$ was first dissolved in 25.0 mL of distilled water in a glass beaker, followed by the addition of 25.0 mL of a $CaCl_2$ aqueous solution (0.2 M) drop by drop under magnetic stirring at room temperature. The mixture was kept under stirring for about 10 min, and then 50.0 mL of a NaF aqueous solution (0.2 M) was added into 12.5 mL of the mixture suspensions and stirred for another 10 min. Excess NaF was used to ensure the complete conversion of $CaWO_4$ into CaF_2. The resulting suspension was maintained at room temperature for 5 days without stirring and shaking. The products were collected by centrifugation, washed several times with distilled water and absolute ethanol, and finally dried in air at 60 °C for 1 h.

X-ray diffraction (XRD) patterns were recorded on a Rigaku D/max-rA diffractometer with Cu Kα radiation ($\lambda = 1.5406$ Å). Scanning electron microscopy (SEM) images were taken on Hitachi S-4700 and CamScan MX 2600 field-emission scanning electron microscopes. TEM characterization was carried out on a Phillips Tecnai 20 microscope at an accelerating voltage of 200 kV. High-resolution TEM (HRTEM) characterization and selected area electron diffraction (SAED) patterns were performed on a JEOL3010 microscope at an accelerating voltage of 300 kV, equipped with an X-ray energy-dispersive spectrometer. For TEM and HRTEM experiments, the as-synthesized powders were first dispersed in ethanol by ultrasonic treatment. Then a small drop of the dispersions was transferred to a holey carbon film supported on a copper grid. N_2 adsorption–desorption isotherms were performed on a Micrometrics ASAP 2020 V3.00 H system with N_2 as the analysis gas after the sample was degassed in a vacuum at 120 °C overnight. The pore diameter and pore-size distribution at the shell were determined by the Barrett–Joyner–Halenda (BJH) method.

3. RESULTS AND DISCUSSION

The phase and purity of the as-obtained CaF_2 hollow microspheres are characterized by XRD, as shown in Figure 1c. The strong and sharp diffraction peaks indicated that the as-obtained CaF_2 hollow microspheres are well-crystallized. All of the diffraction peaks of the XRD pattern can be

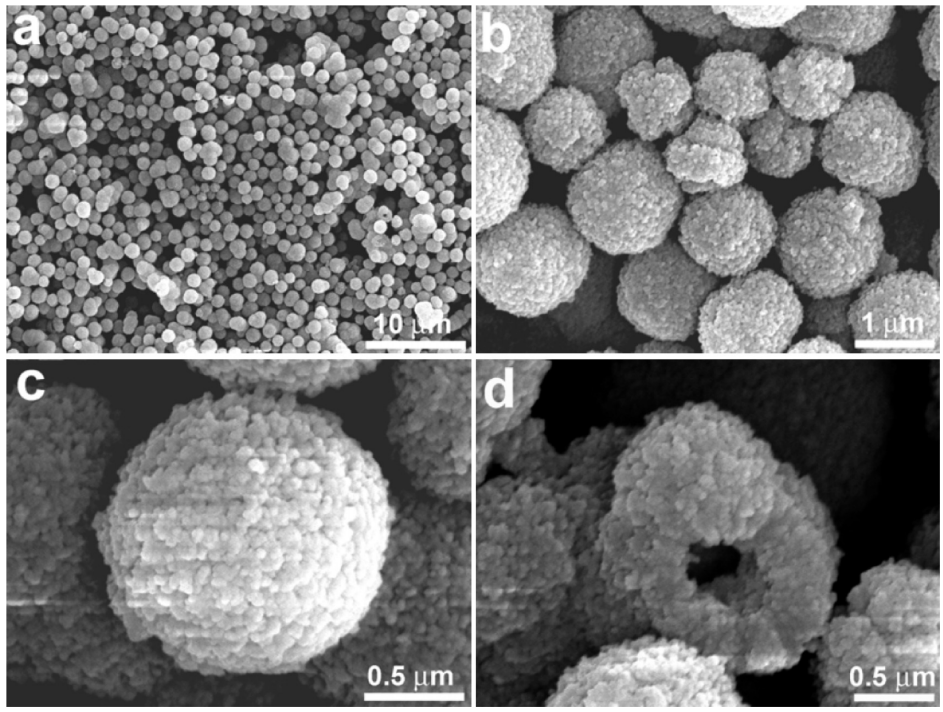

FIGURE 2. (a) Low- and (b) high-magnification SEM images of the as-synthesized CaF_2 hollow microspheres. (c) Intact CaF_2 microsphere. (d) Broken CaF_2 microsphere.

perfectly indexed to a pure cubic phase of CaF_2 (JCPDS 77-2096), with a lattice constant of $a = 5.462$ Å. No peaks from $CaWO_4$ are detected from the XRD pattern, which confirms the complete transformation of $CaWO_4$ to CaF_2. The broadening of these diffraction peaks indicates that the CaF_2 hollow microspheres are constructed of small particles. According to the Scherrer equation, the mean size of the CaF_2 particles is estimated to be about 20 nm from the half-widths of the major diffraction peaks.

The panoramic morphologies of the as-synthesized CaF_2 hollow microspheres are examined by SEM, as shown in Figure 2. Figure 2a is a low-magnification SEM image of the sample, which indicates that the product is composed of large-scale microspheres. The proportion of microspheres in the sample is almost 100%. Most of the micropsheres exhibit monodispersive characteristics, although a few microspheres are attached to each other to form large microsphere aggregates. From the enlarged SEM image (Figure 2b), the microspheres have a diameter distribution ranging from 1.2 to 1.8 μm, with an average diameter of 1.5 μm. Figure 2c shows a typical individual CaF_2 microsphere with a diameter of 1.5 μm, exhibiting the detailed structure information of the microspheres. The peripheral surface of the microsphere is not smooth. Interestingly, the microsphere is actually composed of hundreds of nanoparticles with diameter of about 20 nm. Thus-prepared CaF_2 microspheres are very stable, and even long-time ultrasonication could not break them into discrete nanoparticles, suggesting that the microspheres are integrative, not made up of loosely aggregated nanoparticles. Figure 2d shows a broken CaF_2 microsphere of 1.3 μm diameter observed occasionally after ultrasonication. A cavity is observed clearly in the center of the microsphere, which provides direct evidence that the CaF_2 microspheres have a hollow structure. This CaF_2 microsphere has a hollow interior with ~350 nm size and a shell thickness of ~500 nm. The broken microsphere further demonstrates that the shell is composed of numerous nanocrystals. Figure S1 (Supporting Information) also shows some typical broken CaF_2 microspheres after ultrasonication, which clearly displays the hollow interior.

The morphology and structure of the as-synthesized CaF_2 hollow microspheres are further characterized using TEM, SAED, and HRTEM. Figure 3a shows a typical TEM image of the as-prepared CaF_2 microspheres, which shows well-defined monodispersed spheres with an average diameter of about 1.5 μm, in agreement with SEM observations. A strong contrast difference between the dark edges and pale centers indicates that each CaF_2 microsphere has a hollow interior in the center. The hollow interiors have diameters of about 500 nm, and the thickness of the shell is estimated to be about 500 nm (Figure 3b). Figure 3c is a magnified TEM image from the edge of an individual microsphere, revealing that the shell of CaF_2 hollow spheres is composed of numerous tiny nanocrystals with diameters of about 20 nm. The corresponding SAED pattern (inset in Figure 3c) depicts that the shell is polycrystalline in nature because the shell is composed of nanocrystals. Figure 3d shows the HRTEM image of a single nanoparticle from the shell of the microsphere. The clear lattice image indicates the single-crystalline nature of the CaF_2 nanocrystals. A lattice spacing of 0.27 nm for the (200) plane of the cubic CaF_2 structure can be readily resolved. The chemical compositions of the as-synthesized CaF_2 hollow microspheres are checked using energy-dispersive spectrometry (EDS), as shown in Figure 3e. The EDS spectrum shows the presence of Ca and F peaks with an approximate stoichiometry of CaF_2, together with a Cu signal

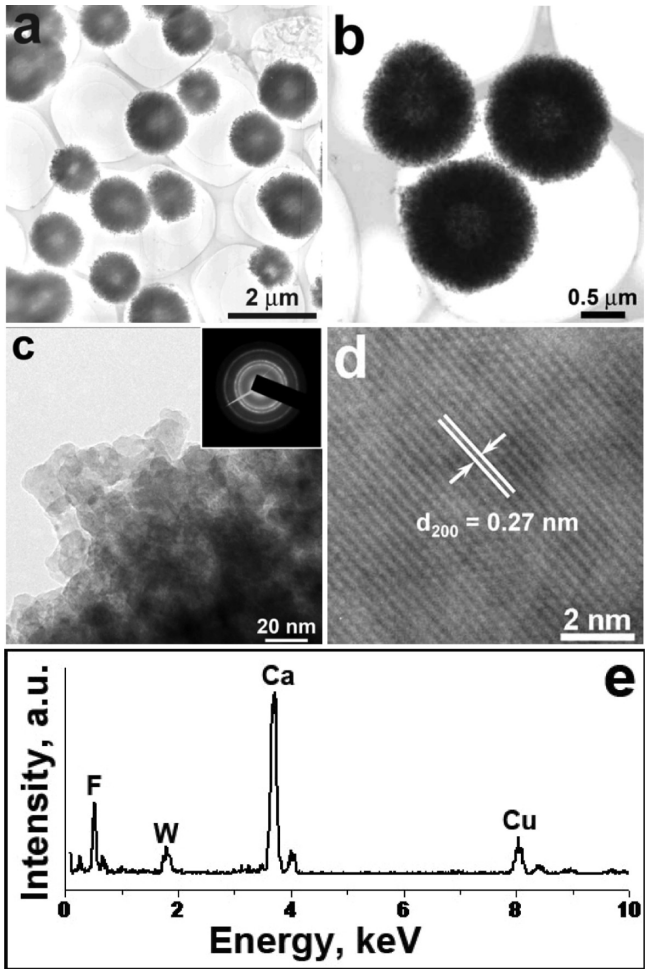

FIGURE 3. (a) Low- and (b) high-magnification TEM images of the as-synthesized CaF_2 hollow microspheres. (c) High-magnification TEM image of the shell from the hollow microspheres and its corresponding SAED pattern as the inset. (d) HRTEM image of an individual nanocrystal taken from the shell of the microsphere. (e) EDS spectrum of the as-synthesized CaF_2 hollow microspheres.

coming from the TEM grid and low-W intensity. Quantitative analysis shows that the content of W is only 0.4 atom %. The EDS result further demonstrates that the main composition of the as-obtained product is CaF_2. Furthermore, it can also be detected from the contrast in the enlarged TEM image that there exist interstitials in the sphere's shell (Figure S2 in the Supporting Information). On the basis of the previous study, this novel hollow structure represents an ideal candidate for potential applications. For example, this hollow interior can act as a good container for many functional guest materials, while the interstitials between the sphere's shells will enable guest materials traveling in or out to work as "nanochannels" for material exchange between the interior and exterior of the spheres (1f, 11, 19).

To develop a comprehensive understanding of the synthesis of the CaF_2 hollow microspheres, a series of contractive experiments are carried out, and the results indicate that the concentration of the aqueous NaF solution and the reaction temperature play important roles in controlling the morphology of the final CaF_2 products. Figure 4 shows typical SEM images of CaF_2 products obtained at varied concentrations of the aqueous NaF solution. When the concentration of the aqueous NaF solution is decreased from 0.2 to 0.12 M while keeping the other reaction conditions the same as those for a typical synthesis, CaF_2 spherical aggregates are produced, as shown in Figure 4a,b. The microspheres have diameters of 1.5−2.5 μm, and most of the microspheres tend to form irregular chainlike aggregates. When the reaction is carried out at a relatively higher concentration of the aqueous NaF solution (0.4 M), SEM images (Figure 4c,d) show that the product contains CaF_2 microspheres with diameters of about 2 μm, together with lots of crashed or irregular microparticles. As the concentration of the aqueous NaF solution is further increased to 1 M, large quantities of CaF_2 cubes with size of about 500 nm are synthesized, coexisting with CaF_2 microspheres 2 μm in diameter (Figure 4e,f). From these SEM images, it is revealed that only an appropriate concentration of the aqueous NaF solution of about 0.2 M is indispensable for the formation of near-monodisperse CaF_2 hollow microspheres with narrow diameter distribution. The reaction temperature is also an important factor affecting the morphologies of the CaF_2 products. For the CaF_2 sample synthesized at 40 °C, large-scale irregular microspheres with diameters of about 2 μm are obtained (Figure 5a). The high-magnification SEM image shows that most of the microspheres are attached to each other to form large microsphere aggregates of several microns in size, as shown in Figure 5b. Interestingly, no microspheres but only nanoparticles with diameters of 50−100 nm are synthesized when the reaction temperature is increased to 80 °C, as shown in Figure 5c,d. It is obvious that the concentration of the reaction reagents and the reaction temperature have significant effects on the formation process of CaF_2 hollow microspheres, which will be discussed below.

To explore the formation mechanism of the CaF_2 hollow microspheres, two controlled experiments were further carried out. The first experiment was carried out in the absence of the NaF aqueous solution. Without the addition of the aqueous NaF solution to the reaction system, monodispersive $CaWO_4$ solid microspheres with an average diameter of 3 μm were obtained when an aqueous $CaCl_2$ solution was added into the aqueous Na_2WO_4 solution at room temperature, as shown in Figure 6. The other experiment was carried out by the direct reaction between aqueous $CaCl_2$ and NaF solutions at room temperature for 5 days without using Na_2WO_4 (the concentrations of aqueous $CaCl_2$ and NaF solutions are both 0.2 M). No crystalline precipitation of CaF_2 was obtained in this condition. These controlled experimental results indicate that the formation process of CaF_2 in our study contains two steps: first the formation of $CaWO_4$ solid microspheres and then their conversion to CaF_2. The formation of $CaWO_4$ solid microspheres from the reaction between aqueous $CaCl_2$ and Na_2WO_4 solutions plays an important role in the final growth of CaF_2 microspheres, where $CaWO_4$ microspheres might act as both the calcium source to release Ca^{2+} ions and the structure director in the formation of CaF_2 microspheres in the reaction system.

Generally, inorganic colloidal crystals are preferred as in situ sacrificial templates in the fabrication of other inorganic

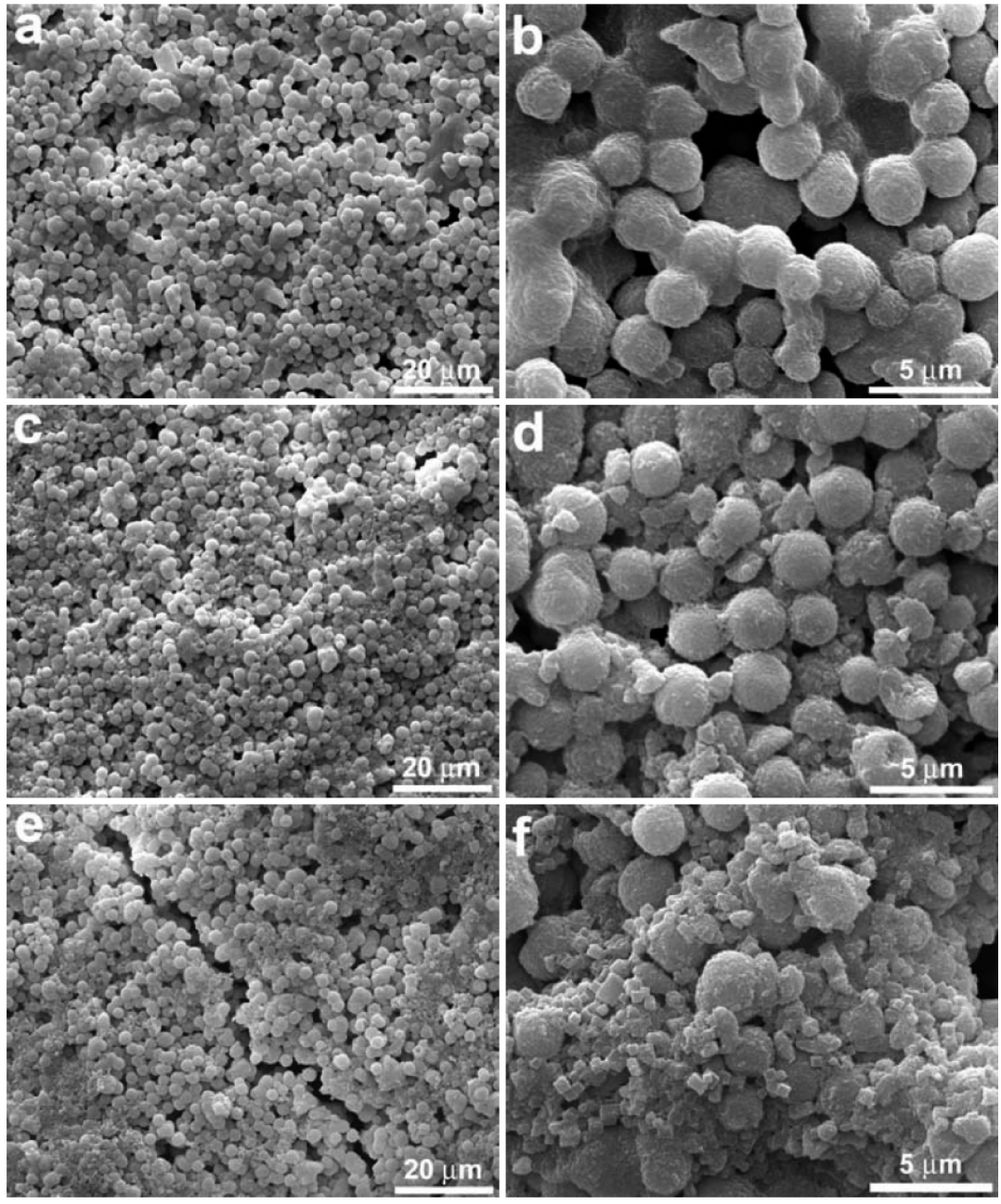

FIGURE 4. SEM images of the CaF_2 products prepared in the presence of different concentrations of NaF: (a and b) 0.12 M; (c and d) 0.4 M; (e and f) 1 M.

colloidal nanostructures involving an ion-exchange reaction, where a large solubility product (K_{sp}) is a key reference for direct replacement between two kinds of materials (20). In the reaction system, the following three reactions are believed to be responsible for the formation of CaF_2 microspheres: (1) $Ca^{2+} + WO_4^{2-} = CaWO_4$; (2) $CaWO_4 = Ca^{2+} + WO_4^{2-}$; (3) $Ca^{2+} + 2F^- = CaF_2$. $CaWO_4$ microspheres are first obtained through the direct reaction between $CaCl_2$ and Na_2WO_4 aqueous solutions, as shown in reaction 1. When the NaF aqueous solution is introduced, the conversion from $CaWO_4$ to CaF_2 is possible because of the K_{sp} difference for $CaWO_4$ and CaF_2 (K_{sp} for $CaWO_4 = 8.7 \times 10^{-9}$; K_{sp} for $CaF_2 = 2.7 \times 10^{-11}$) at room temperature. The $CaWO_4$ microspheres can be in situ dissociated slowly to release the Ca^{2+} ions in the reaction system when F^- ions are introduced (reaction 2). Thus, the anion-exchange reaction between WO_4^{2-} and F^- ions spontaneously takes place to form CaF_2 when the Ca^{2+} ions meet with F^- ions (reaction 3). In addition, using excess F^- ions as anion ions in our reaction system is also favorable for the formation of CaF_2 microspheres because the equilibrium of reaction 3 will shift right naturally, as indicated by Le Chatelier's principle. On the basis of the above discussion, the formation of $CaWO_4$ microspheres as the reaction intermediate templates initiates the growth of CaF_2 microspheres.

It is well-known that complex morphologies of inorganic materials are usually difficult to produce by directly mixing two aqueous solutions of metal salts because of a rapid decrease in supersaturation and further depletion of the reaction nutrients in a short period of time (21). However,

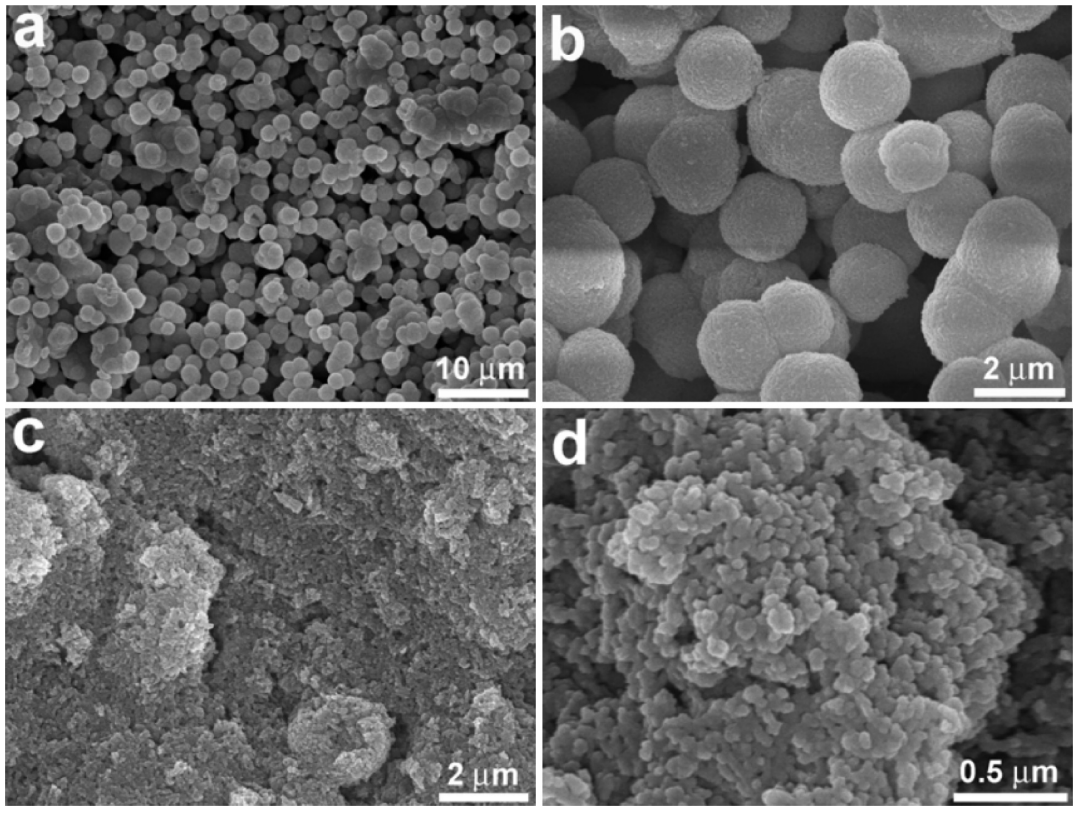

FIGURE 5. SEM images of CaF_2 products synthesized at different reaction temperatures: (a and b) 40 °C; (c and d) 80 °C.

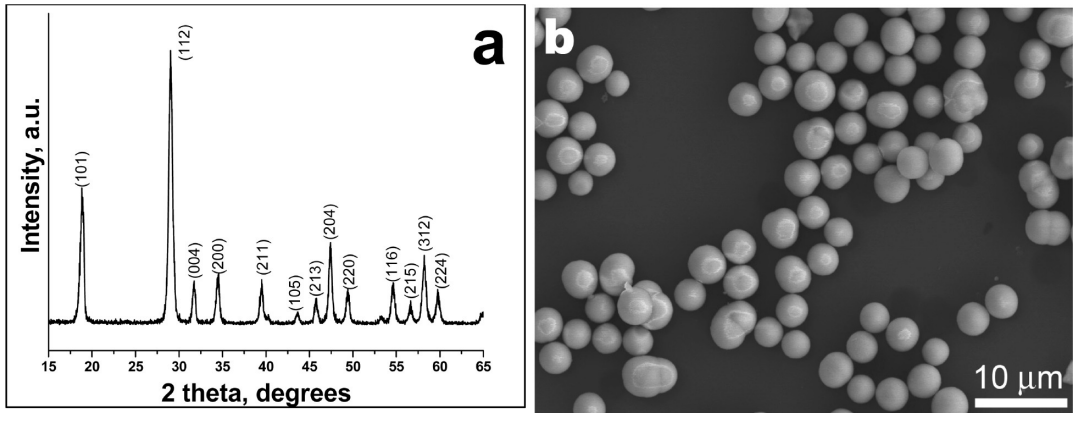

FIGURE 6. (a) XRD pattern and (b) SEM image of the as-synthesized $CaWO_4$ microspheres before the addition of the NaF aqueous solution into the reaction system.

in the present reaction system, using the reaction intermediate, $CaWO_4$ microspheres, as the precursor might slowly release Ca^{2+} ions into the solution and lead to a suitable reaction rate for generation of CaF_2, which might provide a favorable chemical environment for the growth of CaF_2 micropsheres composed of nanoparticles. Compared with the direct reaction between aqueous $CaCl_2$ and NaF solutions, the reaction velocity in our reaction system can be adjusted through the $CaWO_4$ slow-release Ca^{2+} method, which can regulate the kinetics of the nucleation and growth of the products and further efficiently control the morphology and structure of the final products.

To obtain a better understanding of the formation of CaF_2 hollow microspheres, time-dependent experiments were carried out while keeping the other reaction conditions the same. Several experiments through interception of the intermediate products were performed at precipitation stages of 1, 24, and 72 h. The intermediate products were inspected by TEM, as shown in Figure 7. Parts a and b of Figure 7 present the TEM images of the sample obtained after a reaction time of 1 h, in which only monodispersive solid microspheres and no hollow spheres are obtained. The XRD patterns corresponding to intermediate products obtained at precipitation stages of 1 h are shown in Figure 1a. All of the diffraction peaks of the XRD pattern can be indexed to a cubic phase of CaF_2 (JCPDS 77-2096). The EDS spectrum (Figure S3 in the Supporting Information) taken from the microsphere also shows that the chemical composition of the microsphere is CaF_2 even after a short reaction time of 1 h. A Further high-magnification TEM image shows that the

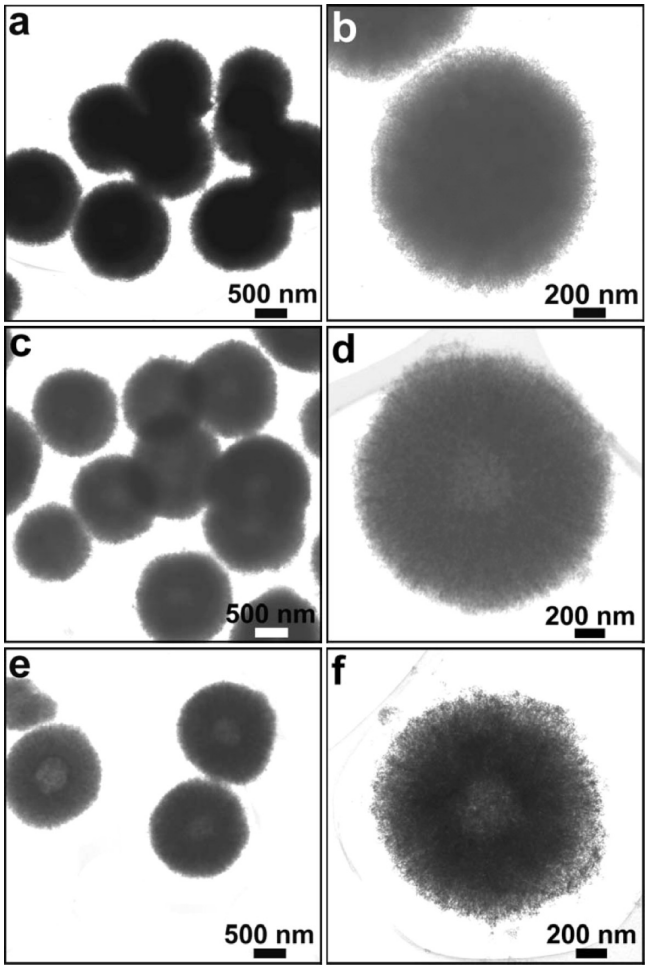

FIGURE 7. TEM images of the samples obtained at different precipitation stages at room temperature showing the hollowing process: (a and b) 1 h; (c and d) 24 h; (e and f) 72 h.

solid microsphere is composed of numerous single-crystalline CaF_2 nanoparticles (Figure S4a,b in the Supporting Information). The corresponding SAED pattern (Figure S4c in the Supporting Information) depicts that the sphere is polycrystalline in nature because the sphere is composed of numerous nanocrystals. When the reaction time is prolonged to 24 h, the close TEM observations (Figure 7c,d) show that the contrast of the core section of these microspheres is quite a bit weaker than that of their exterior part, indicating the existence of a hollow interior. The XRD pattern of the intermediate products obtained at a precipitation stage of 24 h is shown in Figure 1b, which also indicates that the microspheres are CaF_2. Therefore, the phase of the CaF_2 microspheres does not change with a further increase in the reaction time, but the microspheres are followed by a solid core evacuation process. When the reaction duration is prolonged to 72 h, a clearer hollow interior appears in the center of the microsphere (Figure 7e,f). Finally, after the reaction time is further prolonged to 5 days, phase-purity CaF_2 hollow microspheres are obtained on a large-scale, as shown in Figure 1c and 3. Figure S5 in the Supporting Information shows the (111) diffraction peak of CaF_2 samples with a different reaction time. It can be seen that the width of the diffraction peak gradually becomes narrow with

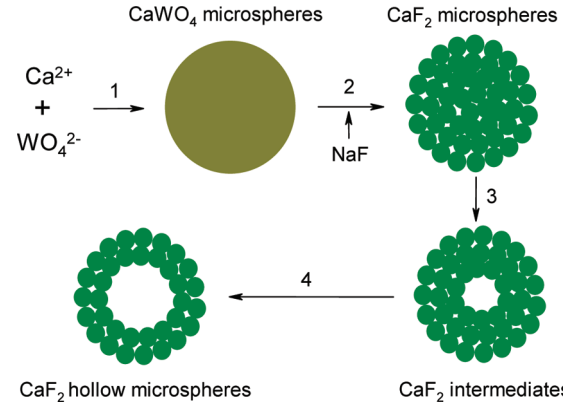

FIGURE 8. Formation process of the CaF_2 hollow microspheres based on the chemical transformation process induced Ostwald ripening mechansim using $CaWO_4$ microspheres as precursors to react with the aqueous NaF solution at room temperature.

increasing reaction time, which suggests that the crystallinity is enhanced with increasing reaction time.

On the basis of above analysis, the formation mechanism of CaF_2 hollow microspheres is believed to be the result of the Ostwald ripening mechanism induced by a chemical transformation of $CaWO_4$ to CaF_2. The Ostwald ripening process mode was first proposed by Zeng et al. in the formation of TiO_2 hollow nanospheres (11), which is further demonstrated in the formation of hollow spheres of γ-MnS (22a), α-MnO_2 (22b), Co_3O_4 (22c), Cu_2O (22d), $CaCO_3$ (22e), $CdMoO_4$ (18b), CuO/Cu_2O composite hollow microspheres (22f), $Cd(OH)_2$ hollow microspheres (22g), $CaWO_4$ hollow microspheres (22h), copolymer−Co hybrid hollow spheres (22i), and so forth. The possible formation mechanism of CaF_2 hollow spheres is also shown by the schematic diagram in Figure 8. In the beginning (Figure 8, step 1), a Na_2WO_4 aqueous solution is mixed with a $CaCl_2$ solution to rapidly produce $CaWO_4$ microspheres at room temperature (Figure 6). Because the K_{sp} of CaF_2 is much lower than that of $CaWO_4$ at room temperature, the chemical transformation of $CaWO_4$ to CaF_2 is possible, where the K_{sp} difference is the main driving force. Because of the strong reaction driving force resulting from the K_{sp} difference between $CaWO_4$ and CaF_2,, chemical transformation occurred and finished even at a reaction time of 1 h (Figures 1a, 7a,b, and S3 in the Supporting Information) when the aqueous NaF solution was introduced into the $CaWO_4$ microspheres suspension (Figure 8, step 2). It should be mentioned that there was no central hollow space in the CaF_2 microspheres formed at this stage, and creation of the central hollow interior would be started only after the above chemical transformation. With a further increase in the reaction time, the CaF_2 microspheres are followed by a solid core evacuation. The TEM observations (Figure 7) illustrate that the hollowing process is essentially similar to what has been known in the preparation of pure anatase TiO_2 hollow spheres (11) and Sn-doped TiO_2 hollow nanospheres (23). After chemical transformation of $CaWO_4$ to CaF_2, these initially formed solid CaF_2 microspheres constructed by numerous nanocrystals might not be well crystallized owing to rapid ion-exchange reaction, and thus Ostwald ripening dictates the growth and recrystallization

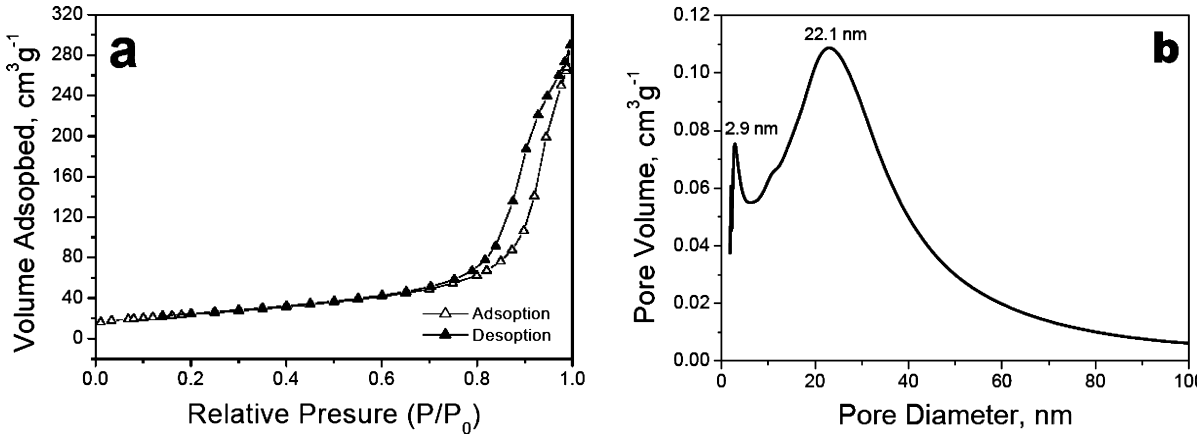

FIGURE 9. (a) N_2 absorption and desorption isotherms and (b) pore-size distributions for the as-synthesized CaF_2 hollow microspheres.

with enough ripening time. According to the XRD results shown in Figure 1, the width of the diffraction peak gradually becomes narrow with an increase in the reaction time, which also demonstrates that the crystallinity is enhanced with an increase in the reaction time. Previous studies have demonstrated that the Ostwald ripening process will happen during this time because smaller, less crystalline, or less dense particles in a colloidal aggregate will be dissolved gradually while larger, better crystallized, or denser particles in the same aggregate grow (11, 23). During this ripening process, the inner crystallites would dissolve and transfer out, producing channels connecting the inner and outer spaces in the CaF_2 shells (Figure 8, step 3) (24). The cores could be further excavated with enough ripening time owing to the higher surface energy. Once the cores in the center of the microspheres are consumed completely, the hollow microspheres are formed (Figure 8, step 4). During this hollowing process, the diameters of the intermediate products intercepting in different reaction stages of 1, 24, and 72 h do not change much, which is similar to what has been observed in the preparation of TiO_2 (11) and Sn-doped TiO_2 hollow nanospheres (23).

Naturally, there is therefore an important question that remains unanswered. Why is the diameter of CaF_2 less than that of $CaWO_4$ after chemical transformation controlled by the large K_{sp} difference between $CaWO_4$ and CaF_2. After conversion of $CaWO_4$ to CaF_2, the reduction in the diameter can be attributed to the fact that the density of CaF_2 (3.18 g/cm^3) is relatively lower than that of $CaWO_4$ (6.38 g/cm^3), which results in a decrease of the diameter (25). Because the density of CaF_2 is much lower than that of $CaWO_4$, there will be a significant volume contraction for CaF_2 after conversion from $CaWO_4$. Therefore, there will be a decrease in the volume when $CaWO_4$ is converted to CaF_2.

It should be pointed out that, during the chemical transformation induced Ostwald ripening mechanism-based synthesis of CaF_2 hollow microspheres, the most important factors influencing the morphologies and sizes are the concentration of the aqueous NaF solution and the reaction temperature. On the basis of the above discussion, the effect of the concentration of the aqueous NaF solution on the morphology of CaF_2 samples is mainly due to the mass diffusion between $CaWO_4$ and CaF_2 in the aqueous solutions. According to Fick's first law, the varied concentration of the aqueous NaF solution will change the concentration gradient of F^- ions in the reaction solution, which will subsequently affect the mass (F^- ions) following the chemical transformation of $CaWO_4$ to CaF_2 solid spheres. When the concentration of NaF is 0.12 M, the concentration gradient of F^- ions in the solution is decreased compared with that of 0.2 M, which will lead to a decrease in mass (F^- ions) flowing per unit time, resulting in irregular chainlike CaF_2 microspherical aggregates (Figure 4a,b). When the concentration of NaF is increased to 0.4 M (or higher, 1 M), the concentration gradient of F^- ions in the solution will be increased and the mass (F^- ions) flowing per unit time will increase. The diffusion of F^- ions and sequentially generated CaF_2 nuclei will be accelerated, resulting in CaF_2 nanocubes as byproducts (Figure 4c–f). Therefore, the reactant concentration exerts an important impact on the crystal nucleation and growth, which is responsible for the morphology of the products. Similar to the concentration of the aqueous NaF solution, a high temperature will also accelerate the diffuse process, especially at 80 °C, leading to the growth of microspherical aggregates and nanoparticles. Therefore, a suitable concentration of the aqueous NaF solution and the reaction temperature will provide a favorable chemical environment for the diffuse balance between $CaWO_4$ and CaF_2, resulting in CaF_2 hollow microspheres based on the chemical transformation induced Ostwald ripening process.

To investigate the specific surface area and porous nature of the hollow CaF_2 microspheres, BET gas-sorption measurement is carried out. The recorded N_2 adsorption–desorption isotherms for the product show significant hysteresis at relative pressures P/P_0 above 0.6 (Figure 9a). The hysteresis loop can be categorized as type IV, which is the characteristic of mesporous materials. The BET surface area of the sample is about 85.7 m^2/g calculated from N_2 isotherms at 77 K. Feldmann et al. have reported that the specific area of CaF_2 nanocrystals is 78.6 m^2/g (17a). The CaF_2 hollow microspheres obtained here have an extremely high BET area. BJH calculations for the pore-size distribution reveal a narrow distribution apex centered at 2.9 and 22.1 nm, respectively (Figure 9b). The pores are possibly attributed to the inter-

nanocrystal spaces, which is in agreement with TEM observation (Figure 3c). The results indicate that the obtained CaF_2 hollow microspheres have excellent porous properties.

4. CONCLUSIONS

In summary, we have demonstrated a simple aqueous solution route for large-scale synthesis of CaF_2 hollow microspheres from a mixture of aqueous solutions of $CaCl_2$, Na_2WO_4, and NaF at room temperature. The formation of $CaWO_4$ solid microspheres plays important roles in the final growth of CaF_2 microspheres, where $CaWO_4$ solid microspheres might act as both the calcium source to release Ca^{2+} ions and the structure director in the formation of CaF_2 microspheres in the reaction system. The formation mechanism for the CaF_2 hollow microspheres is related to the chemical transformation induced Ostwald ripening mechanism based on time-dependent experiments. The obtained CaF_2 hollow micropsheres have excellent porous properties. Taking into account a harmless and low-cost synthetic procedure, high BET surface area, and favorable porous characterization, CaF_2 hollow microspheres developed in the present work are promising candidates for technical applications in areas of material encapsulators or carriers, biocompatible luminescent markers, and optical nanodevices.

Acknowledgment. This work was supported by the Natural Scientific Research Innovation Foundation of the Harbin Institute of Technology (Grant HIT.NSRIF.2008.32). We thank Miaomiao Ye at the Harbin Institute of Technology for skillful measurement during the BET gas-sorption experiment.

Supporting Information Available: SEM images of CaF_2 hollow microspheres, TEM images of CaF_2 hollow micropsheres, TEM and HRTEM images, SAED pattern, and EDS results of the CaF_2 solid microspheres at a reaction time of 1 h, and XRD patterns CaF_2 micropsheres. This material is available free of charge via the Internet at http://pubs.acs.org.

REFERENCES AND NOTES

(1) (a) Caruso, F.; Caruso, R. A.; Mohwald, H. *Science* **1998**, *282*, 1111. (b) Jiang, P.; Bertone, J. F.; Colvin, V. L. *Science* **2001**, *291*, 453. (c) Im, H. S.; Jeong, U.; Xia, Y. N. *Nat. Mater.* **2005**, *4*, 671. (d) Yin, Y. D.; Rioux, R. M.; Erdonmez, C. K.; Hughes, S.; Somorjai, G. A.; Alivisatos, A. P. *Science* **2004**, *304*, 711. (e) Jeong, U.; Wang, Y. L.; Ibisate, M.; Xia, Y. N. *Adv. Funct. Mater.* **2005**, *15*, 1907. (f) Lou, X. W.; Yuan, C. L.; Zhang, Q.; Archer, L. A. *Angew. Chem., Int. Ed.* **2006**, *45*, 3825. (g) Zeng, H. C. *J. Mater. Chem.* **2006**, *16*, 649. (h) Schwartzberg, A. M.; Olson, T. Y.; Talley, C. E.; Zhang, J. Z. *J. Phys. Chem. B* **2006**, *110*, 19935. (i) Low, X. W.; Archer, L. A.; Yang, Z. C. *Adv. Mater.* **2008**, *20*, 3987. (j) Wang, W. S.; Zhen, L.; Xu, C. Y.; Shao, W. Z. *Prog. Chem.* **2008**, *20*, 679.

(2) (a) Jachson, J. B.; Halas, N. J. *J. Phys. Chem. B* **2001**, *105*, 2743. (b) Velikov, K. P.; Blaaderen, A. V. *Langmuir* **2001**, *17*, 4779. (c) Wang, Y.; Su, F. B.; Lee, J. Y.; Zhao, X. S. *Chem. Mater.* **2006**, *18*, 1347.

(3) (a) Caruso, F.; Shi, X.; Caruso, R. A.; Susha, A. *Adv. Mater.* **2001**, *13*, 740. (b) Lu, Y.; McLellan, J.; Xia, Y. N. *Langmuir* **2004**, *20*, 3464.

(4) Sun, X. M.; Li, Y. D. *Angew. Chem., Int. Ed.* **2004**, *43*, 3827.

(5) (a) Gao, J.; Zhang, B.; Zhang, X.; Xu, B. *Angew. Chem., Int. Ed.* **2006**, *45*, 1220. (b) Sun, Y.; Mayers, B.; Xia, Y. N. *Adv. Mater.* **2003**, *15*, 641.

(6) Bruinsma, P. J.; Kim, A. Y.; Liu, J.; Baskaran, S. *Chem. Mater.* **1997**, *9*, 2507.

(7) Yang, H. G.; Zeng, H. C. *Angew. Chem., Int. Ed.* **2004**, *43*, 5206.

(8) Li, Y.; Shi, J.; Hua, Z.; Che, H.; Ruan, M.; Yan, D. *Nano Lett.* **2003**, *3*, 609.

(9) (a) Fowler, C. E.; Khushalani, D. D.; Mann, S. *Chem. Commun.* **2001**, 2028. (b) Fowler, C. E.; Khushalani, D. D.; Mann, S. *Chem. Commun.* **2001**, 2028. (c) Gao, X.; Zhang, J.; Zhang, L. *Adv. Mater.* **2002**, *14*, 290.

(10) Huang, J. X.; Xie, Y.; Li, B.; Liu, Y.; Qian, Y. T.; Zhang, S. Y. *Adv. Mater.* **2002**, *12*, 808.

(11) Ma, Y. R.; Qi, L. M.; Ma, J. M.; Cheng, H. M. *Langmuir* **2003**, *19*, 4040.

(12) (a) Peng, Q.; Dong, Y.; Li, Y. D. *Angew. Chem., Int. Ed.* **2003**, *42*, 3027. (b) Guo, L.; Liang, F.; Wen, X. G.; Yang, S. H.; He, L.; Zheng, W. Z.; Chen, C. P.; Zhong, Q. P. *Adv. Funct. Mater.* **2007**, *17*, 425.

(13) Zeng, H. C. *Curr. Nanosci.* **2007**, *3*, 177.

(14) Yang, H. G.; Zeng, H. C. *J. Phys. Chem. B* **2004**, *108*, 3492.

(15) (a) Singh, R.; Sinha, S.; Chou, P.; Hsu, N. J.; Radpour, F. *J. Appl. Phys.* **1989**, *66*, 6179. (b) Quan, Z. W.; Yang, D. M.; Yang, P. P.; Zhang, X. M.; Lian, H. Z.; Liu, X. M.; Lin, J. *Inorg. Chem.* **2008**, *47*, 9509.

(16) (a) Moon, H. J.; Kim, K. N.; Kim, K. M.; Choi, S. H.; Kim, C. K.; Kim, K. D.; LeGeros, R. Z. *J. Biomed. Mater. Res., Part A* **2005**, *74*, 497. (b) Kumar, G. A.; Chen, C. W.; Riman, R.; Chen, S.; Smith, D.; Ballato, J. *Appl. Phys. Lett.* **2005**, *86*, 241105. (c) Pilvi, T.; Arstila, K.; Leskela, M.; Ritala, M. *Chem. Mater.* **2007**, *19*, 3387.

(17) (a) Feldmann, C.; Roming, M.; Trampert, K. *Small* **2006**, *2*, 1248. (b) Zhang, X. M.; Quan, Z. W.; Yang, J.; Yang, P. P.; Lian, H. Z.; Lin, J. *Nanotechnology* **2008**, *19*, 075603. (c) Sun, X. M.; Li, Y. D. *Chem. Commun.* **2003**, 1768. (d) Mao, Y. B.; Zhang, F.; Wong, S. S. *Adv. Mater.* **2006**, *18*, 1895.

(18) (a) Wang, W. S.; Xu, C. Y.; Zhen, L.; Yang, L.; Shao, W. Z. *Chem. Lett.* **2006**, *35*, 268. (b) Wang, W. S.; Zhen, L.; Xu, C. Y.; Zhang, B. Y.; Shao, W. Z. *J. Phys. Chem. B* **2006**, *110*, 23154. (c) Wang, W. S.; Zhen, L.; Xu, C. Y.; Zhang, B. Y.; Shao, W. Z. *J. Nanosci. Nanotechnol.* **2008**, *8*, 1288. (d) Wang, W. S.; Zhen, L.; Xu, C. Y.; Yang, L.; Shao, W. Z. *Crystal Growth Des.* **2008**, *8*, 1734.

(19) Jia, B. P.; Gao, L. *J. Phys. Chem. C* **2007**, *112*, 666.

(20) (a) Sun, Y. G.; Wiley, B.; Li, Z. Y.; Xia, Y. N. *J. Am. Chem. Soc.* **2004**, *126*, 9399. (b) Jeong, U.; Kim, J.; Xia, Y. N. *Nano Lett.* **2005**, *5*, 937. (c) Zhu, W.; Wang, W. Z.; Shi, J. L. *J. Phys. Chem. B* **2006**, *110*, 9785.

(21) Zhang, Z.; Shao, X.; Yu, H.; Wang, Y.; Han, M. *Chem. Mater.* **2005**, *17*, 332.

(22) (a) Zheng, Y. H.; Cheng, Y.; Wang, Y. S.; Zhou, L. H.; Bao, F.; Jia, C. *J. Phys. Chem. B* **2006**, *110*, 8284. (b) Li, B. X.; Rong, G. X.; Xie, Y.; Huang, L. F.; Feng, C. Q. *Inorg. Chem.* **2006**, *45*, 6404. (c) Liu, B.; Zeng, H. C. *Small* **2005**, *1*, 566. (d) Chang, Y.; Teo, J. J.; Zeng, H. C. *Langmuir* **2005**, *21*, 1074. (e) Yu, J. G.; Guo, H. T.; Davis, S. A.; Mann, S. *Adv. Funct. Mater.* **2006**, *16*, 2035. (f) Yu, H. G.; Yu, J. G.; Liu, S. W.; Mann, S. *Chem. Mater.* **2007**, *19*, 4327. (g) Wang, W. S.; Zhen, L.; Xu, C. Y.; Shao, W. Z. *J. Phys. Chem. C* **2008**, *112*, 14360. (h) Wang, W. S.; Zhen, L.; Xu, C. Y.; Shao, W. Z. *J. Phys. Chem. C* **2008**, *112*, 19390. (i) Qiao, R.; Zhang, X. L.; Qiu, R.; Kim, J. C.; Kang, Y. S. *Chem. Mater.* **2007**, *19*, 6485.

(23) Li, J.; Zeng, H. C. *J. Am. Chem. Soc.* **2007**, *129*, 15839.

(24) Lou, X. W.; Wang, Y.; Yuan, C. L.; Lee, J. Y.; Archer, L. A. *Adv. Mater.* **2006**, *18*, 2325.

(25) Jeong, U.; Kim, J.-U.; Xia, Y. N.; Li, Z. Y. *Nano Lett.* **2005**, *5*, 937.

AM8002044